Adaptive Optics for Photoreceptor-Targeted Psychophysics

17

Wolf M. Harmening and Lawrence C. Sincich

17.1 Seeing Cells of the Retina

The eye has a clear advantage over other sensory organs when it comes to directly observing its neurosensitive structures non-invasively, for it is already built as an image forming system. The eye's large aperture and transparent cornea and lens allow a nearly unobstructed view of the retina lining the back of the globe, where the neuronal tissue resides and can be seen with even simple optical instruments. In this chapter we will focus on a relatively recent experimental approach that makes use of that access to study the human retina at the most elementary level of the single cone photoreceptor. By directly linking targeted stimulation of individual photoreceptors to subjective visual perception in psychophysical experiments, visual processing mechanisms operating at the cellular level in the retina can be uncovered.

The technological hurdles to be overcome for cell-based psychophysics were achieved by building upon continued innovations in ophthalmoscopic imaging. Ophthalmoscopy, a field devoted to viewing the inside of the eye, began with the invention of the direct ophthalmoscope in 1851 by Hermann von Helmholtz, and initiated a close relationship between imaging innovations with ever increasing fidelity on the one hand and milestone discoveries in vision research and clinical ophthalmoscopy on the other [1]. From the onset, Helmholtz noted the optical imperfections in the eye that make closer examination challenging [2]. Due to natural irregularities in shape and refractive index of the optical media, the eye introduces optical aberrations that fundamentally limit the quality of the acquired images in an ophthalmoscope [3]. Nevertheless, in eyes with minimal native aberrations, single photoreceptors can be readily observed. By taking photographs of the retina through the pupil of their eyes, the first *in vivo* images of the photoreceptor mosaic were produced in animals with especially large receptors, the garter snake (*Thamnophis* spp.) [4] and cane toad (*Bufo marinus)* [5]. The first *in vivo* images of human photoreceptors were captured with a custom digital fundus camera [6]. Here, a key prerequisite to seeing single cells was a careful correction of defocus and astigmatism to sufficiently improve the optical quality of the image forming process.

Concurrently, other technological breakthroughs in retinal imaging were the development of optical coherence tomography (OCT) [7], and the scanning laser ophthalmoscope (SLO) [8]. While OCT readily creates cross-sectional

W. M. Harmening (✉)
Department of Ophthalmology, University of Bonn, Bonn, Germany

L. C. Sincich
Department of Optometry and Vision Science, University of Alabama at Birmingham, Birmingham, AL, USA

images of the retina along the optical axis in an interferometric approach, confocal SLO technology allows *en face* images of the retina by detecting backscattered light reflected from a transverse plane of the retina. Both OCT and SLO are able to resolve the retinal mosaic of photoreceptor cells in young eyes with clear ocular media when both defocus and astigmatism are minimal, and typically at perifoveal retinal locations where the photoreceptors are in the range of 8 μm in diameter [9, 10]. Similar near diffraction-limited resolution in eyes with more demanding natural aberrations was only achieved by equipping ophthalmoscopy with a set of tools first developed in astronomy to improve the resolution of ground-based telescopes: adaptive optics (AO) [11–13] (see also Chap. 16).

The core of an AO system is an adjustable wavefront correcting element, typically a deformable mirror, and was first implemented in an SLO in 1989 [14]. Without a wavefront sensor, correction of previously determined low order aberrations (defocus and astigmatism) could be performed; however, image quality did not improve by a large margin, mostly because higher order aberrations were still left uncorrected, a prominent issue when the imaging beam fills the aperture of a dilated pupil. A key advance was introduced in 1994 by employing a Shack-Hartmann wavefront sensor to continuously measure ocular aberrations [15], and the first AO-ophthalmoscope that was able to correct higher order aberrations based on measurement of the ocular wavefront in closed-loop operation was demonstrated in 1997 [16]. The introduction of adaptive optics in ophthalmoscopy marked the birth of a new generation of high resolution retinal imaging devices, and today, 20 years after its first appearance, AO for the eye is available, partly commercially, in three main imaging modalities: fundus photography [16, 17], optical coherence tomography [18, 19], and scanning laser ophthalmoscopy [20, 21].

Here we provide an overview of an experimental approach that uses adaptive optics combined with scanning laser ophthalmoscopy (AOSLO) to study the function of individual photoreceptors in the human retina. AOSLO systems are primarily deployed in experimental and clinical research settings to study microscopic retinal structure with high lateral resolution, and as such, are often used as a pure imaging system [13, 22, 23]. An AOSLO can also be utilized as a microscopic stimulation platform where controlled amounts of light are briefly flashed at precise retinal locations to stimulate an area approaching the size of a single photoreceptor while a subject responds in a psychophysical task [24, 25]. This specific experimental technique has emerged during the last 10 years, and there is currently no other method available with comparable optical precision, spatial control of delivered stimuli, and freedom in experimental options.

In the following sections we will first briefly review key retinal factors that have an impact on retinal image formation and vision before we turn to the optical and technical requisites needed to experimentally control the activity of single cone photoreceptors seen during AOSLO imaging. We will then illustrate a few empirical findings, to demonstrate what can be learned about the visual system in healthy and diseased retinas when photoreceptor function is probed *in vivo*.

17.2 Retinal Factors Interacting with Photoreceptor Imaging and Function

Photoreceptors are the first cells that transform the stream of photons impinging on the retina into neurochemical signals that mediate vision to the brain [26, 27]. The photoreceptors sit in the most posterior layer of the retina. Consequently all incoming light has to travel through the overlying retinal tissue comprised of blood vessels and a dense network of neurons and interneurons before it can be absorbed for the use of vision. Here we briefly review pertinent aspects of the retina's cellular composition and how it interacts with the incoming light before we delve into how visual function can be approached by the activation of single photoreceptors.

As the light sensitive neuronal tissue of the eye, the human retina lines the inner walls of
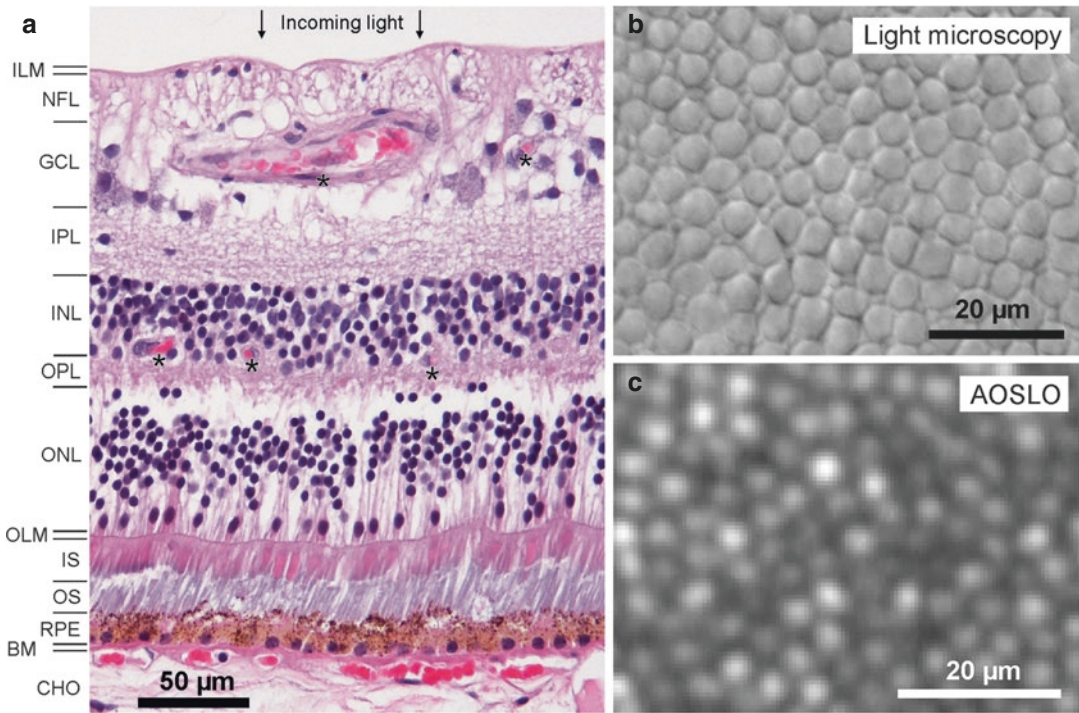
Fig. 17.1 The retina and photoreceptor mosaic. (**a**) Hematoxylin and eosin stain of a human retina in cross section. Light entering the eye (arrows) passes through dense layers of neuronal cells and blood vessels (asterisks) before it is absorbed in the outer segments of the photoreceptors. *ILM* inner limiting membrane, *NFL* nerve fiber layer, *GCL* ganglion cell layer, *IPL* inner plexiform layer, *INL* inner nuclear layer, *OPL* outer plexiform layer, *ONL* outer nuclear layer, *OLM* outer limiting membrane, *IS* photoreceptor inner segments, *OS* photoreceptor outer segments, *RPE* retinal pigment epithelium, *BM* Bruch's membrane, *CHO* anterior part of the choroid. (**b**) In a macaque retinal flat mount at ~3° eccentricity (~0.6 mm away from the foveal center) photographed with differential interference contrast microscopy, cone inner segments are visible as closely packed circular structures, interspersed with a few smaller rod inner segments. (**c**) *In vivo* AOSLO imaging of cones from another macaque, also at 3° eccentricity. Rods are unresolved in this image, but are likely to be nestled in the dark gaps between cones

the globe. Except around the fovea where it is thicker, most of the retina is ~300 μm in depth, containing three prominent cell body layers, two extensively interwoven synaptic layers, and four membranous layers (Fig. 17.1a). From anterior to posterior, following the light as it enters the eye, these strata are: (1) the inner limiting membrane, a thin Müller-cell derived layer separating the vitreous body from the retina; (2) the nerve fiber layer containing ganglion cell axons that carry the retinal signals to the brain; (3) the ganglion cell layer of ~one million cells consisting of more than 20 functionally distinct cell classes; (4) the inner plexiform layer, a synaptic network funneling bipolar and amacrine cell signals onto the ganglion cells; (5) the inner nuclear layer, containing the cell bodies of bipolar, amacrine, Müller, and horizontal cells; (6) the outer plexiform layer, formed by the synapses between multiple bipolar cell classes and photoreceptors; (7) the outer nuclear layer of the rod and cone photoreceptor cell bodies; (8) the outer limiting membrane, an epithelial structure providing mechanical strength; and finally (9) the photoreceptor inner and outer segments, the latter being where phototransduction takes place upon the absorption of light by the photopigments. The outer segments are embedded in the retinal pigment epithelium, a single layer of polygonal, highly pigmented cells, serving to absorb uncaptured light and carry out important phagocytotic functions of the visual cycle.

When light hits the eye, it has to pass through all anterior retinal layers before it is absorbed at the cone outer segments. Some of these layers introduce considerable light distortion, a fact that is capitalized on in OCT, where backscattered light is used to produce a useful cross section of the retina [7]. For AOSLO imaging and microstimulation, some of these light-tissue interactions are critical, and can be readily observed in the images collected. The most prominent sources of light distortion are the vessels of the inner retinal vasculature (Fig. 17.1a), manifesting as cast shadows in AOSLO images of the photoreceptor layer. It has been shown that cones that sit in such shadows have reduced sensitivity [28] and that the spectral sensitivity of penumbral cones is changed compared to their open-field neighbors [29]. The nerve fiber layer also scatters strongly and can be visualized in confocal AOSLO images [30], but its impact on cone targeted stimulation lights is yet unknown.

The strongest signal in AOSLO images stems from reflections originating in the photoreceptor layer (Fig. 17.1b, c). Each retina of a human eye carries an average of 92 million rod photoreceptors and 4.6 million cone photoreceptors [31]. These cells are unequally distributed in the retina, with foveal cones reaching an average peak density of ~200,000 cells/mm^2 (declining rapidly to less than 10,000 cells/mm^2 at ~6° eccentricity) while rod density peaks at ~150,000 cells/mm^2 near 10° eccentricity, with none in the fovea itself. Rods are just about uniformly sized at 2 μm diameter (at the inner segment) and respond to single photon absorptions, making them the foundation of scotopic vision [32, 33]. Many rods make contact with the same target bipolar cell, thus their combined output is amplified by signal convergence. In contrast, cones vary in size with eccentricity, from a foveal minimum of ~1.5 to ~8 μm at larger eccentricities. Phototransduction is more rapid in cones than in rods and is less sensitive, requiring ~50 photon absorptions to trigger a threshold response [34]. Cone mediated vision is specialized for high resolution, both temporally, to detect fast image motion, and spatially, for high acuity tasks. In trichromatic animals such as humans, each cone carries one of three types of photopigment that have distinct absorption maxima within the visible spectrum, and are hence called long (L), medium (M), and short (S) wavelength sensitive cones. The spatial arrangement of these cone classes is surprisingly variable in every retina, and were first revealed in human eyes using AO imaging [35, 36].

The cellular structure of the retina is probably one of the best studied sensory tissues, yet its functional architecture is still subject to active scientific investigation, in part because it is relatively difficult to study in the intact organism. What we will see in the next section is that by coupling AOSLO imaging to cone-targeted microstimulation, light can be shed on retinal function all the way from pre-receptor optical factors (such as the geometry of light capture by cone outer segments), to post-photoreceptor factors (such as horizontal cell feedback), and finally to visual perception (such as spatial and color vision).

17.3 Resolving and Targeting Individual Photoreceptors for Visual Function Testing

Studying retinal function can be done in many ways, with perhaps the simplest being the brief presentation of a spot of light somewhere in the visual field and asking the subject or patient "Did you see it?" With some added degree of spatiotemporal control, this is how one of the most fundamental visual function tests, perimetry, is performed in a standard clinical examination. In clinical perimetry as well as in most psychophysical studies of visual function, many photoreceptors are stimulated simultaneously even when small spots of light are used (e.g. Goldmann size I, 6.5 arcmin), and the visual percept is necessarily a product of summed receptor activity. When the goal is to characterize the function of individual photoreceptors the task becomes more challenging. Cell-resolved visual function testing demands that single photoreceptors are probed selectively. To target a single receptor, it needs to be visible, and in order to perform psychophysical testing the cell has to be stimulated

with light repeatedly while limiting any light that might land on neighboring receptors [37]. Here we will discuss the main optical, physiological, and technical challenges that arise from doing such experiments, how they can be overcome, and what insights about vision can be discovered with a single cell targeted approach.

17.3.1 Monochromatic Aberration Correction

For cell-resolved retinal imaging and stimulation, optical challenges arise because the eye itself introduces a number of optical imperfections. Foremost of these is the optical quality of the dioptric apparatus of the eye, formed by the cornea and intraocular lens. These tissues are made up of cells that grow into place during development, and since such biological processes cannot always form perfectly, the lens and cornea do not mature with an optically ideal shape. Indeed, human eyes manifest particular lower and higher order monochromatic aberrations caused by irregularities in shape and refractive power of these structures [38]. Rays of light traversing the eye will thus be refracted irregularly, causing optical distortions that ultimately limit the quality of the retinal image. With small pupils, image blur due to diffraction outweighs aberrations, and the resolution of the eye is closer to diffraction limited. A larger pupil on the other hand adds to diffraction blur the many distortions related to ocular aberrations that are prominent when the incoming beam passes through larger portions of the cornea and lens [39]. As all current AO imaging systems use a large beam to achieve the best retinal imaging, having a correspondingly large pupil (via pharmaceutically induced dilation) sweeps in all these aberrations that need to be compensated.

For ophthalmoscopic imaging of the human eye, the limiting aperture is the pupil, the nearly circular opening formed by the iris, a muscular extension of the ciliary body, which can take on diameters anywhere between ~1 and 8 mm. This pupil sets the lateral resolution limit for imaging, typically defined mathematically by the point spread function (PSF). Assuming a perfect optical system, the form of the eye's PSF would be solely governed by diffraction, and therefore is a function of wavelength and optical aperture size (see also Chap. 19). It is here where we face a trade-off: large pupils allow higher spatial resolution (smaller PSFs) but at the same time increase the extent of ocular aberrations that need to be corrected. The latter hurdle is overcome by AO, enabling good resolution with aberrations minimized.

In a real eye, optical quality is also significantly reduced by factors other than dioptrics. Light scattering within the ocular media and tissues have to be considered, especially when aiming to deliver spatially restricted light to photoreceptors. Some degree of forward light scattering occurs within each of the tissues lying in the path in front of the photoreceptors, while light that reflects from tissues behind the photoreceptors will also diffuse small stimuli. Both types of scattering are considered straylight and will cause the ocular PSF to broaden and hence reduce contrast of retinal images [40, 41]. The amount of straylight is only weakly correlated with pupil size [42]. With current optical techniques, even AO, straylight cannot be compensated for and so will cause some portion of the light in micron-scale stimuli to be captured by non-targeted photoreceptors.

It should now be clear that the goal of an AO system for ophthalmic imaging is to reduce the contribution of monochromatic aberrations to approach diffraction limited lateral resolution while keeping within physiological pupil sizes [13, 43]. Correcting ocular aberrations is achieved by an optical element that can flexibly alter the wavefront of the beam entering the eye. This is typically achieved with either a deformable mirror or a liquid crystal spatial light modulator. Deformable mirrors can take on complex shapes due to mechanical deflection by an array of linear actuators [44]. Alternatively, liquid crystal light modulators can be used to alter the phase point-by-point of a transmitted beam [45]. In both cases, the phase of the incoming wavefront is locally adjusted to create a flattened wavefront when the beam is reflected from the back of the

eye. Of course, this requires that the wavefront be known. There are several ways to measure the wavefront aberrations of the eye, and the most commonly used is a Shack-Hartmann sensor, an image sensor placed behind an array of micro lenses ([15], see also Chap. 16). Here, a beam of light reflected from the retina is imaged onto the lenslet array and the focused spots behind each lens are analyzed. Any offset in this array of spots from a perfect orthogonal grid indicate a distortion in wavefront shape. This error signal can be used to drive the corrective elements of a deformable mirror or light modulator to create a compensatory wavefront shape, either in a continuous closed-loop fashion, or discontinuous open-looped mode with repeated measurements [46]. Ocular wavefronts can also be measured via surface plasmon excitation with a pair of highly sensitive CCD sensors [47]. There are also sensorless methods, where wavefront corrections are emplaced directly from the acquired retinal image quality in an iterative algorithmic process [48].

For retinal imaging, AO is employed in three main imaging modalities: flood illumination ophthalmoscopy [16], in combination with an SLO [20, 21], or with OCT [18, 19]. All three modalities have complementary advantages for retinal imaging and all are of great clinical relevance since microscopic retinal structures become visible in the living subject [49–51]. These structures include the retinal nerve fiber layer and lamina cribrosa [22], blood flow with single blood cell resolution in the smallest capillaries [52–54], individual cone and rod photoreceptors [10, 55–57], retinal ganglion cells [58, 59], and the mosaic of the retinal pigment epithelium [60, 61]. For visual stimulation, the AOSLO is able to produce stimuli with the highest spatial precision. This is because imaging and stimulation can be spatially and temporally coupled within the same beam in an SLO [62–64].

17.3.2 Stimulus Light Modulation and Image Motion Compensation

Another set of concerns for cone-targeted stimulation is how to control when and where the stimulus will be delivered to the retina, and how to account for the often substantial retinal motion. In an AOSLO, images of the photoreceptor mosaic are created by collecting the reflected light from a focused beam that is raster scanned across a small square area on the retina over time (Fig. 17.2). This rastered image is produced by orthogonally deflecting the system's beam in a vertical and horizontal fashion. To achieve video frame rates at image sizes of, for example,
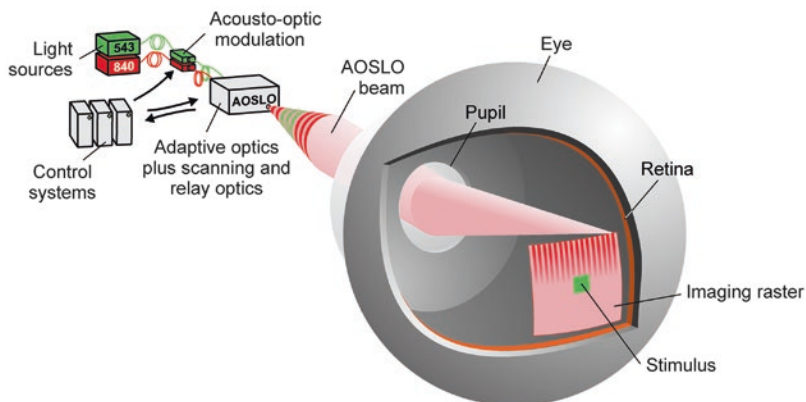
Fig. 17.2 Schematic of AOSLO microstimulation. A visible stimulus is produced by high-speed acousto-optic modulation of a focused beam that is scanned across the retina. Because both imaging and stimulus wavelengths (840 and 543 nm, respectively) travel along the same beam path, stimuli can be positioned with high retinal contingency when eye motion and chromatic offsets have been compensated for by a set of control systems (see text for details)

512×512 pixels, one scan direction operates at 30 Hz, while the orthogonal deflection rate—for a square image aspect ratio—is the product of the numbers of lines in the scan field and the frame scan rate ($512 * 30$ Hz ≈ 16 kHz). To create each video frame, each pixel is rendered by assigning the temporal signal in the light detectors to a spatial coordinate that corresponds to the current position of the imaging beam within the raster. The spatio-temporal relationship between beam position and acquired image pixel is not linear, because the high scan frequencies needed for the fast scan axis are produced by sinusoidal travel of a resonant scanning mirror. This means that the time needed for the beam to traverse the retinal space that corresponds to a single image pixel varies with beam position, with slower speeds close to the reversal points of each scan line. These sinusoidal distortions can be corrected by recording an image of an equi-spaced grid mounted in a model eye and then de-sinusoiding any ocular images on- or offline to achieve isotropic pixels in the captured frame [65, 66].

Retinal stimulation can be achieved in a multi-wavelength AOSLO by passing the imaging and stimulus light through independent acousto-optic modulators (AOMs) prior to their entry into the scanning and corrective portions of the optical path. Stimulus lights can thus be modulated in concurrence and with high spatial contingency to the retinal image. This correspondence allows custom stimuli to be delivered to the retina—pixel by pixel—at selectable locations within the imaging raster [67]. One difficulty for repeated stimulation at the same retinal location is that even if a subject's head is perfectly immobilized in front of the fixed beams of an AOSLO, any retinal locus remains an ever-moving target. This is due to the eye being in constant motion, even during steady fixation [68, 69]. While the subject is not aware of fixational eye movements and their amplitudes are small, they are large compared to the size of single photoreceptors. Typically, any visual stimulus is translated across tens to hundreds of cone photoreceptors during normal viewing [70, 71]. Because of the scanning nature of the AOSLO, the consequences produced by these

small eye movements are readily observable and directly measurable in the acquired images [72, 73]. Fast software stabilization algorithms have been developed to measure image strip offsets and to correct the AOM timing signals accordingly [74, 75]. With this real-time stabilization of fixational eye movements, stimulus positions can be locked onto selected retinal locations, with a residual position jitter of about 0.15 arcmin, an area slightly smaller than the diameter of the smallest photoreceptors [76]. Saccades and microsaccades are too large to be corrected at present, so they must be ignored, or at least recognized when they occur in order to reject any compromised data.

Due to the enormous dynamic range of human photoreceptors in response to light, studying their visual function across that range is challenging because standard visual stimulation devices such as LCD monitors have limited luminance contrasts that can be displayed. By cascading two commercially available fiber-coupled acousto-optic modulators (AOMs), i.e. feeding the output of one AOM to the input of a second AOM, a multiplicative extinction ratio can be achieved. Single light switch events as short as 50 ns with radiant power contrasts up to $1:10^{10}$ were demonstrated [77], which essentially spans the normal dynamic range of cone photoreceptors. Psychophysically, this contrast ratio was shown to be sufficient to stimulate single foveal photoreceptor cells with small and bright enough visible targets that do not contain a detectable background light. Background-free stimulation allows testing with custom adaptation lights, and the larger dynamic range in displayable light levels can drive photoreceptor responses in cones as well as in the scotopic regime of rod photoreceptors.

17.3.3 Chromatic Dispersion Compensation

To provide more freedom in stimulation options, AOSLO systems are designed with separate imaging and stimulation wavelengths [78, 79]. Typically, near-infrared wavelengths are used

for imaging because of the high retinal reflectivity of that part of the spectrum (we should note that at the powers required to image the retina, this infrared light is often visible as a deep red square), while shorter visible wavelengths are used for stimulation, especially when color phenomenon are being investigated. Because the refractive power of the eye varies as a function of wavelength, this requires consideration of the effects of chromatic dispersion. Chromatic dispersion in the ocular media causes light of different wavelengths to focus in different axial planes and at different locations in the transverse plane, effects termed longitudinal chromatic aberration (LCA) and transverse chromatic aberration (TCA), respectively [80]. LCA has been shown to be relatively consistent between individuals, and can be compensated for by adjusting the relative vergence angles of the fiber optic point sources as they enter the system [79]. The direction and magnitude of TCA is more idiosyncratic, and depends on the position of the imaging and stimulation beams relative to the eye's achromatic axis [81, 82] and is not centered on the pupil [83]. Typical lateral shifts of beam positions due to TCA can easily exceed the diameter of single cones, thus it has to be carefully corrected for cone targeted stimulation. Because transverse beam position shifts can be directly measured by comparing the images formed with the employed wavelengths in the AOSLO, the combined effects of TCA and spatial offsets between imaging and stimulus beams can be compensated for each subject and for every eye position individually [79]. One consequence of this approach is that a significant amount of light (e.g. equaling a luminance of ~50,000 cd/m^2 in 543 nm) is required to capture retinal images with the visible wavelengths. In practice, chromatic offset measurements have thus to be performed before or after psychophysical experiments, because these light levels are too bright for concurrent stimulation and to allow visual adaptation to return to normal states. This intermittent measurement leaves some uncertainty whether correction was performed accurately during an experiment, and thus the use of a bite bar to restrict head movements to a minimum is advised [24].

17.3.4 Cone Targeted Psychophysics

Finally, the combination of the technological innovations described in the preceding sections have enabled the study of *in vivo* psychophysical responses when single cones or groups of cones have been targeted for stimulation. Even when one cone is targeted for stimulation, it must be recognized that there is always a small fraction of the light that will fall on nearby cones, a fraction that is hard to measure. The stimulus uncertainties are mainly due to residual uncorrected aberrations, stimulus delivery errors, and uncontrolled scatter [37]. Nevertheless, some key advances have been made in our understanding of how visual perception is driven by the selective activation of single photoreceptors, and we will briefly review them here.

As a first proof-of-principle, psychometric functions of sensitivity to light increments have been recorded in normal subjects when cone-sized stimuli were targeted at single parafoveal cone centers or at the space between them (Fig. 17.3) [24]. It was found that thresholds could be measured reliably when such stimuli where delivered to the same cone. Moreover, when the light was intentionally targeted to the space between cones, thresholds rose substantially, directly demonstrating that the light capturing capabilities of the retina are spatially discrete. Modeling the light sensitivity of small groups of cones like that in Fig. 17.3a as Gaussian light apertures showed that some stimulus blur remained, ~0.06 D, but this is likely due to uncertainty about the exact focal position that yields the best AOSLO imaging. The basic result suggests that the spatial grain of perception is constrained by the exact arrangement of cones in any patch of retina and the exact placement of stimuli onto those waveguiding cones.

An unexplained observation in all confocal AOSLO images is that cone reflectivity varies to a large degree, from moment to moment and from day to day in the same subject. Could these differences in cone reflectivity be linked to differences in light capture? To test this idea, pairs of cones—one appearing bright, one dark— were stimulated with randomly interleaved trials
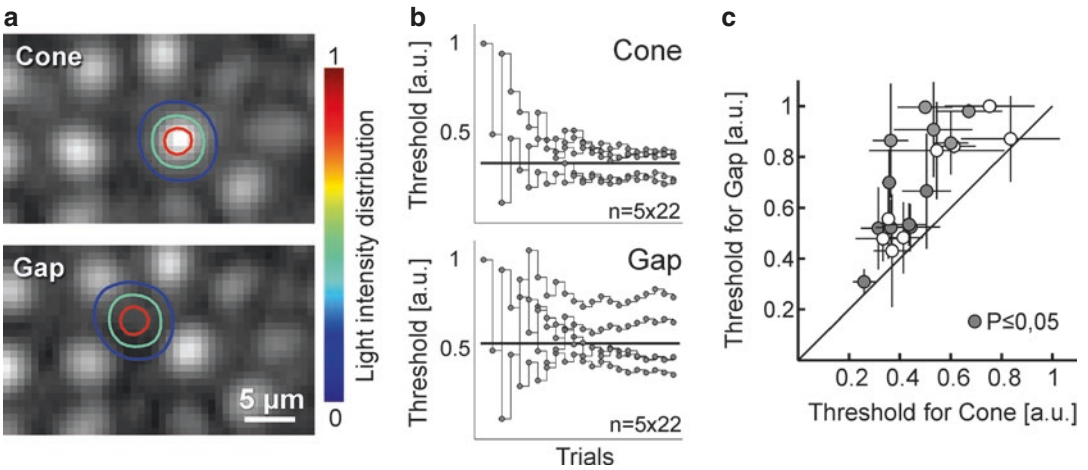
Fig. 17.3 Increment threshold sensitivity to cone-sized stimuli. (**a**) Perceptual responses can be measured when stimuli are targeted at one cone photoreceptor (top), or at the space between them (bottom). Contour lines represent the relative light distribution of spot stimuli after repeated trials (n = 22). (**b**) An increment sensitivity threshold can be measured for each location with an adaptive staircase, shown here as five runs at the same location (horizontal line = mean threshold value from all runs). Note that more light was needed (higher threshold) to detect the stimulus when it was targeted at the space between cones. (**c**) The positional effect of stimulus placement on sensitivity was shown in four subjects at various locations, with a mean cone-to-gap ratio of 1.3. Data published in [24]
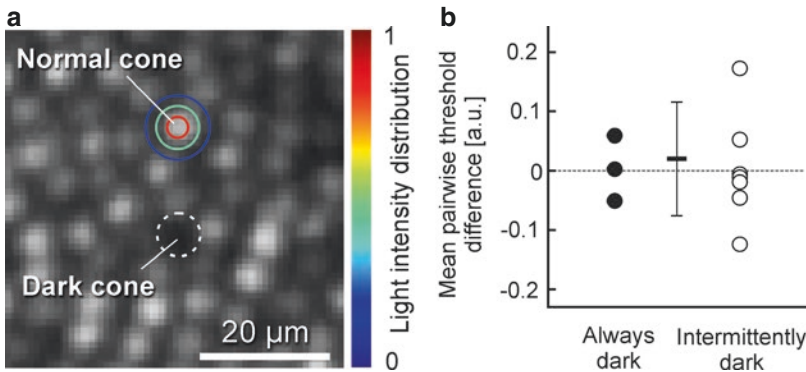
Fig. 17.4 Cone sensitivity is unrelated to reflectivity. (**a**) Example cone pair tested as described in the text for threshold sensitivity, one normally reflective (beneath stimulus light intensity contours) and one relatively dark (dashed outline). (**b**) Among ten pairs in five subjects, dark cone thresholds were not significantly different from normally reflective cones, when compared to the mean of each pair. Data are shown individually for persistently dark and intermittently dark cones, as classified across many imaging sessions. This result indicates that cone reflectance in AOSLO images is not closely coupled to light absorbing efficacy. Horizontal bar is the mean across all pairs, vertical bars are ±1 SD. Data published in [84]

in five subjects with normal vision, again using an increment sensitivity design to see whether cone reflectance could predict thresholds [84]. In ten such directly tested cone pairs, no relationship between cone brightness and cone sensitivity was found (Fig. 17.4). Moreover, across normally reflective cones studied across several

months and subjects (n = 284 pairs), there was a 3.6% higher threshold in darker cones, but this difference was not significant. This small effect was greatly outweighed by the variability of cone brightness in AOSLO images, and thus appears negligible for any sensitivity tests. The degree of cone reflectivity is known to be

unrelated to cone spectral class, whether L, M, or S [36, 85]. Instead, it is likely that light interference in the waveguiding cone may play a role, possibly related to outer segment length changes as they occur during daily phagocytosis [50, 86].

That single photoreceptors can be stimulated to elicit percepts has been shown by several groups [24, 85, 87]. As we have seen in Sect. 17.2, the cellular network of the retina is, however, a complex circuit, where downstream neurons play key roles in how the visual signals are shaped before they reach conscious interpretation by the brain. Some of these postreceptoral mechanisms are now being studied by AO microstimulation. One example from the realm of spatial vision is visual information pooling. By recording increment sensitivity thresholds from retinal areas decreasing in size down to the single cone, it was shown that even when optical aberrations and eye motion have been minimized, summation areas in the fovea are as predicted by Ricco's law. This suggests that foveal spatial summation is limited by post-receptoral neural pooling with a fixed spatial extent, with parasol ganglion cells being a likely candidate for defining the summation area for the tested stimulus conditions [88]. Direct horizontal cell mediated interactions between cones were tested when cones of known class where stimulated with cone class-biasing adaptation background lights [89]. Here, a group of ~100 cones in each of two color normal subjects where first biophysically classed according to their opsin type to yield a map identifying the L, M, and S cones within a small retinal patch [90]. Next, increment thresholds with different background lights that bias sensitivity towards either L or M cones were measured from each classified photoreceptor. It was found that the composition of cell types in the immediate neighborhood of each targeted cell modulated its sensitivity: if more neighbors were of the opposite type, thresholds were higher. This could be explained by lateral inhibition driven by the background light, likely mediated by horizontal cells, that make negative feedback connections with L and M cones indiscriminately.

Another set of experiments took full advantage of AOSLO microstimulation to examine color sensitivity directly. Color percepts where gauged in subjects while a small monochromatic spot was placed persistently onto one cone, with a wavelength of 543 nm that would equally activate L and M cones. Two color normal observers were asked to name the color perceived. These stimuli, presented against a uniform white background, were targeted at cells which were functionally classed before, and thus the relationship between opsin type (cone class) and color percept could be revealed [85]. Color sensations generated by targeted cones were found to be stable over time, and not inextricably bound to cone type. In addition, both L and M cones more often elicited achromatic than chromatic percepts. These results were consistent with the idea that color and spatial information can flow along separate pathways, beginning from the first synapse in the retina. With a similar experimental design, it was shown that the exact spatial makeup of the cone mosaic and their types has an impact on hue categorization. M cones, more often than L cones, generated blue percepts in the presence of a short-wavelength background, and in one of the two tested subjects, this likelihood was elevated when more S-cones were in the immediate vicinity of the probed M-cone (Fig. 17.5), indicating a direct interaction between these two cone classes [91]. By carefully adjusting the wavelength composition and intensity of the background and intensity of the stimulus light, another study found that color naming and saturation ratings 1.5° from the fovea were highly correlated with cone-type, independent of stimulus spot intensity [92]. Such a result suggests that the visual system offers enough spatial resolution to assign a meaningful hue label to stimulus lights that selectively activate single—functionally colorblind—cones.
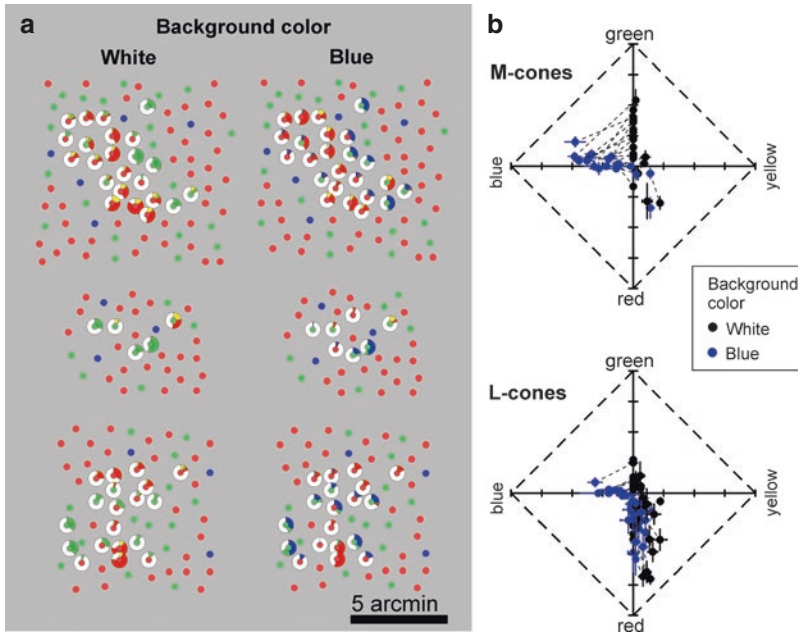
Fig. 17.5 Color perception associated with single cone photoreceptors. (**a**) In one subject at three different locations (rows) where cones have been densitometrically classified (L, M, and S cone locations plotted in red, green and blue), cones where stimulated with a 543 nm cone-sized stimulus against either a white or blue uniform background (columns). Subjective hue scaling responses were recorded and are depicted as ring plots, giving the percentage of responses within the possible hue categories (white, red, yellow, green, blue) at each cone, tested 10 times. (**b**) When a blue background was used, hue percepts shifted towards blue, an effect particularly visible in M cones (top), and less so in L cones (bottom). Error bars are SEM, dashed lines connect responses from one cell. Unpublished data provided by Brian Schmidt, Katharina Foote, Alexandra Boehm and Austin Roorda, UC Berkeley

17.4   Cell-Resolved Vision Testing in Clinical Ophthalmology

With a continuously growing number of studies using AO to image the diseased retina, the ability to see individual photoreceptors in a patient's eye has become a valuable tool in the ophthalmological clinic [22, 23]. With AO imaging, it is apparent that many retinal diseases exhibit structural changes of the photoreceptor mosaic involving cell loss or disruption, often only discernible at the microscopic level. That cell-resolved imaging may be a tool for early detection of latent disease onset holds considerable promise for vision health, and future therapeutic approaches may be identified efficiently with photoreceptor based imaging biomarkers [93, 94].

Translating the ability to study retinal function with AO microstimulation into a clinical setting ought to yield new insights but comes with its own set of complications that need consideration. For patient populations, the primary challenges are poorer image quality due to aged or opaque optical media, increased eye movements due to a disturbance of fixational capabilities, and larger constraints on functional testing time due to limits in a patient's ability to remain in a study chair. Due to its mode of operation, AO wavefront correction depends on reflected light from the retina. With cloudy optical media, e.g. in the presence of a cataract, it is currently not possible to create a correctable wavefront signal, and thus AO offer no advantage over conventional imaging techniques. Because of the much smaller field of view, retinal imaging with an AO system is also much more negatively affected by eye movements, which in turn makes retinally stabilized stimulus delivery difficult. In some forms of ocular disease, such as retinal dystrophies, normal fixational eye movements are accompanied

by large nystagmus-type eye movements [95]. While smaller fixational eye movements can be compensated for by hardware or software based image stabilization tools [76, 96], larger motion amplitudes can be counteracted by active beam steering [96, 97]. An intense pathological nystagmus, however, can considerably prolong the imaging process, degrade image quality, or may render correction impossible completely [43, 56, 98]. Essentially any disease that affects foveal-mediated fixation, such as age-related macular degeneration, is expected to make targeted stimulation challenging, although AO imaging without stimulation could still be performed.

Despite these additional complications, AO microstimulation in retinal disease is an active and growing field of research that has already extended our knowledge about normal and abnormal photoreceptor structure and function. Specific operational features have been developed to help make AO microperimetry more useful for patient testing [28]. In addition to real-time image stabilization, cone test locations can be digitally stored for reuse, making it easier to overcome interruptions during testing and to allow follow-up sessions to be initiated quickly. Psychophysical measurements of cone sensitivities can be time consuming and thus any testing strategy has to be maximized for efficiency. Adaptive staircase procedures such as QUEST have been demonstrated to converge to threshold after about 15-20 trials when testing single cones [24]. The clinically traditional 4–2 dB threshold strategy, as employed in automated perimetry testing for instance, can also be used to quickly converge towards perceptual thresholds, albeit with coarser resolution [99]. The first clinical visual function testing with AO microperimetry was a case of Idiopathic Macular Telangiectasia Type II, a rare early onset disease of the outer retina (Fig. 17.6). In these eyes, in retinal areas where photoreceptors reflected weakly or were not apparent at all, small spot visual sensitivity was found to be normal [100], suggesting that
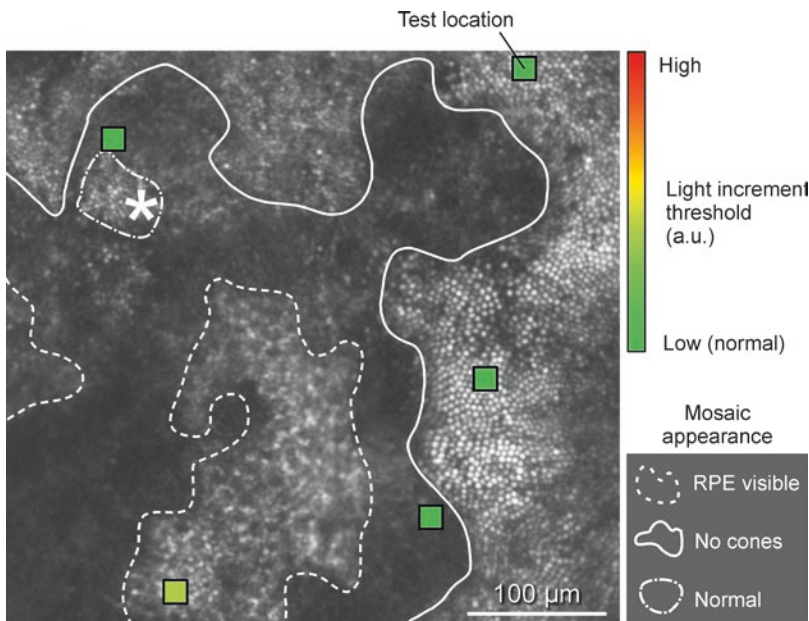
Fig. 17.6 Clinical AOSLO microperimetry. In a patient with Macular Telangiectasia Type II, several retinal locations close to the preferred retinal locus of fixation (asterisk) were tested with AOSLO microstimulation (test locations and stimulus size shown with square markers). Detection threshold for light increments were normal or close to normal in all locations (marker color), despite a markedly disrupted retinal appearance. Areas outside the solid line and inside the dashed-dotted line appear normal with a regular cone mosaic. Areas inside the solid line are hyporeflective, with few discernible cones. Inside the dashed line, the retina is more transparent, showing a mosaic of underlying retinal pigment epithelial cells. Data published in [100]

cones not oriented along the axis of the imaging beam can still retain functionality. This behavior is reminiscent of the finding that dark cones in healthy retinae produce sensitivity thresholds that are indistinguishable from cones with normal reflectivity [84], and that some cones that are dysflective in AOSLO and OCT images convey normal visual sensitivity in a case of acute bilateral foveolitis [101]. Taken together, these first studies of clinical conditions demonstrate that the relationship between cone images and cellular function is not straightforward, and that structural information alone is insufficient to characterize the functional integrity of the retina, especially in cases of retinal disease. Psychophysical or biophysical cell-targeted function testing is likely to become an important adjunct to imaging in order to arrive at a clearer picture of normal as well as disease status in the human retina [24, 102, 103].

References

1. Keeler CR. The ophthalmoscope in the lifetime of Hermann von Helmholtz. Arch Ophthalmol. 2002;120(2):194–201. https://doi.org/10.1001/archopht.120.2.194.
2. Helmholtz H von. Die neueren Fortschritte in der Theorie des Sehens. Populäre Wissenschaftliche Vorträge, zweites He. 1871. p. 21–22.
3. Campbell FW, Gubisch RW. Optical quality of the human eye. J Physiol. 1966;186(3):558–78.
4. Land MF, Snyder AW. Cone mosaic observed directly through natural pupil of live vertebrate. Vis Res. 1985;25(10):1519–22. https://doi.org/10.1016/0042-6989(85)90230-5.
5. Jagger WS. Visibility of photoreceptors in the intact living cane toad eye. Vis Res. 1985;25(5):729–31. https://doi.org/10.1016/0042-6989(85)90179-8.
6. Miller DT, Williams DR, Morris GM, Liang J. Images of cone photoreceptors in the living human eye. Vis Res. 1996;36(8):1067–79.
7. Huang D, Swanson EA, Lin CP, Schuman JS, Stinson WG, Chang W, et al. Optical coherence tomography. Science (New York, NY). 1991;254(5035):1178–81. https://doi.org/10.1002/jcp.24872.The.
8. Webb RH, Hughes GW, Delori FC. Confocal scanning laser ophthalmoscope. Appl Opt. 1987;26(8):1492–9.
9. M, Baumann B, Götzinger E, Hitzenberger CK. Retinal cone mosaic imaged with transverse scanning optical coherence tomography. Opt Lett. 2006;31(12):1821–3. https://doi.org/10.1364/OL.31.001821.
10. Wade AR, Fitzke FW. In vivo imaging of the human cone-photoreceptor mosaic using a confocal LSO. Lasers Light Ophthalmol. 1998;8(3):129–36.
11. Babcock HW. The possibility of compensating astronomical seeing. Publ Astron Soc Pac. 1953;65(386):229–36. https://doi.org/10.1086/126606.
12. Hardy JW. Active optics: a new technology for the control of light. Proc IEEE. 1978;66(6):651–97. https://doi.org/10.1109/PROC.1978.10992.
13. Williams DR. Imaging single cells in the living retina. Vis Res. 2011;51(13):1379–96. https://doi.org/10.1016/j.visres.2011.05.002.
14. Dreher AW, Bille JF, Weinreb RN. Active optical depth resolution improvement of the laser tomographic scanner. Appl Opt. 1989;28(4):804–8. https://doi.org/10.1364/AO.28.000804.
15. Liang J, Grimm B, Goelz S, Bille JF. Objective measurement of wave aberrations of the human eye with the use of a Hartmann-Shack wavefront sensor. J Opt Soc Am A Opt Image Sci Vis. 1994;11(7):1949–57. https://doi.org/10.1364/JOSAA.11.001949.
16. Liang J, Williams DR, Miller DT. Supernormal vision and high-resolution retinal imaging through adaptive optics. J Opt Soc Am A. 1997;14(11):2884–92.
17. Rha J, Jonnal RS, Thorn KE, Qu J, Zhang Y, Miller DT. Adaptive optics flood-illumination camera for high speed retinal imaging. Opt Express. 2006;14(10):4552–69. https://doi.org/10.1364/OE.14.004552.
18. Hermann B, Fernández EJ, Unterhuber A, Sattmann H, Fercher AF, Drexler W, et al. Adaptive-optics ultrahigh-resolution optical coherence tomography. Opt Lett. 2004;29(18):2142–4. https://doi.org/10.1364/OL.29.002142.
19. Jonnal RS, Kocaoglu OP, Zawadzki RJ, Liu Z, Miller DT, Werner JS. A review of adaptive optics optical coherence tomography: technical advances, scientific applications, and the future. Invest Opthalmol Vis Sci. 2016;57(9):OCT51. https://doi.org/10.1167/iovs.16-19103.
20. Merino D, Loza-Alvarez P. Adaptive optics scanning laser ophthalmoscope imaging: technology update. Clin Ophthalmol. 2016;10:743–55. https://doi.org/10.2147/OPTH.S64458.
21. Roorda A, Romero-Borja F, Donnelly WJI, Queener H, Hebert TJ, Campbell MCW, et al. Adaptive optics scanning laser ophthalmoscopy. Opt Express. 2002;10(9):405–12.
22. Carroll J, Kay DB, Scoles D, Dubra A, Lombardo M. Adaptive optics retinal imaging—clinical opportunities and challenges. Curr Eye Res. 2013;38(7):709–21. https://doi.org/10.3109/02713683.2013.784792.
23. Morgan JIW. The fundus photo has met its match: optical coherence tomography and adaptive optics ophthalmoscopy are here to stay. Ophthalmic Physiol Opt. 2016;36(3):218–39. https://doi.org/10.1111/opo.12289.

24. Harmening WM, Tuten WS, Roorda A, Sincich LC. Mapping the perceptual grain of the human retina. J Neurosci. 2014;34(16):5667–77. https://doi.org/10.1523/JNEUROSCI.5191-13.2014.

25. Rossi EA, Roorda A. The relationship between visual resolution and cone spacing in the human fovea. Nat Neurosci. 2010;13(2):156–7. https://doi.org/10.1038/nn.2465.

26. Lee BB, Martin PR, Grünert U. Retinal connectivity and primate vision. Prog Retin Eye Res. 2010;29(6):622–39. https://doi.org/10.1016/j.preteyeres.2010.08.004.

27. Wässle H. Parallel processing in the mammalian retina. Nat Rev Neurosci. 2004;5(10):747–57. https://doi.org/10.1038/nrn1497.

28. Tuten WS, Tiruveedhula P, Roorda A. Adaptive optics scanning laser ophthalmoscope-based microperimetry. Optom Vis Sci. 2012;89(5):563–74. https://doi.org/10.1097/OPX.0b013e3182512b98.

29. Spitschan M, Aguirre GK, Brainard DH. Selective stimulation of penumbral cones reveals perception in the shadow of retinal blood vessels. PLoS One. 2015;10(4):e0124328. https://doi.org/10.1371/journal.pone.0124328.

30. Takayama K, Ooto S, Hangai M, Arakawa N, Oshima S, Shibata N, et al. High-resolution imaging of the retinal nerve fiber layer in normal eyes using adaptive optics scanning laser ophthalmoscopy. PLoS One. 2012;7(3):1–9. https://doi.org/10.1371/journal.pone.0033158.

31. Curcio CA, Sloan KR, Kalina RE, Hendrickson AE. Human photoreceptor topography. J Comp Neurol. 1990;292(4):497–523. https://doi.org/10.1002/cne.902920402.

32. Rieke F, Baylor DA. Single-photon detection by rod cells of the retina. Rev Mod Phys. 1998;70(3):1027–36. https://doi.org/10.1103/RevModPhys.70.1027.

33. Tinsley JN, Molodtsov MI, Prevedel R, Wartmann D, Espigulé-Pons J, Lauwers M, Vaziri A. Direct detection of a single photon by humans. Nat Commun. 2016;7:12172. https://doi.org/10.1038/ncomms12172.

34. Koenig DE, Hofer HJ. The absolute threshold of cone vision. J Vis. 2011;11(1):1–24. https://doi.org/10.1167/11.1.21.Introduction.

35. Hofer HJ, Carroll J, Neitz J, Neitz M, Williams DR. Organization of the human trichromatic cone mosaic. J Neurosci. 2005a;25(42):9669–79. https://doi.org/10.1523/JNEUROSCI.2414-05.2005.

36. Roorda A, Williams DR. The arrangement of the three cone classes in the living human eye. Nature. 1999;397(6719):520–2. https://doi.org/10.1038/17383.

37. Sincich LC, Sabesan R, Tuten WS, Roorda A, Harmening WM. Functional imaging of cone photoreceptors. In: Kremers J, Baraas R, Marshall N, editors. Human color vision, vol. 26. Cham: Springer International Publishing; 2016. p. 71–104. https://doi.org/10.1007/978-3-319-44978-4_3.

38. Salmon TO, van de Pol C. Normal-eye Zernike coefficients and root-mean-square wavefront errors. J Cataract Refract Surg. 2006;32(12):2064–74. https://doi.org/10.1016/j.jcrs.2006.07.022.

39. Miller DT, Roorda A. Adaptive optics in retinal miscroscopy and vision. In: Bass M, editor. Handbook of optics, vol. III. New York: McGraw-Hill Professional; 2010. p. 15.1–15.30.

40. van den Berg TJTP, Franssen L, Coppens JE. Straylight in the human eye: testing objectivity and optical character of the psychophysical measurement. Ophthalmic Physiol Opt. 2009;29(3):345–50. https://doi.org/10.1111/j.1475-1313.2009.00638.x.

41. Westheimer G, Liang J. Influence of ocular light scatter on the eye's optical performance. J Opt Soc Am A. 1995;12(7):1417. https://doi.org/10.1364/JOSAA.12.001417.

42. Franssen L, Tabernero J, Coppens JE, van den Berg TJTP. Pupil size and retinal straylight in the normal eye. Invest Ophthalmol Vis Sci. 2007;48(5):2375–82. https://doi.org/10.1167/iovs.06-0759.

43. Roorda A, Duncan JL. Adaptive optics ophthalmoscopy. Annu Rev Vis Sci. 2015;1(Sec 3):19–50. https://doi.org/10.1146/annurev-vision-082114-035357.

44. Zhang J, Yang Q, Saito K, Nozato K, Williams DR, Rossi EA. An adaptive optics imaging system designed for clinical use. Biomed Opt Express. 2015;6(6):2120. https://doi.org/10.1364/BOE.6.002120.

45. Mu Q, Cao Z, Li D, Hu L, Xuan L. Liquid crystal based adaptive optics system to compensate both low and high order aberrations in a model eye. Opt Express. 2007;15(4):1946–53. https://doi.org/10.1364/OE.15.001946.

46. Fernández EJ, Iglesias I, Artal P. Closed-loop adaptive optics in the human eye. Opt Lett. 2001;26(10):746–8.

47. Vohnsen B, Valente D. Surface-plasmon-based wavefront sensing. Optica. 2015;2(12):1024. https://doi.org/10.1364/OPTICA.2.001024.

48. Hofer HJ, Sredar N, Queener H, Li C, Porter J. Wavefront sensorless adaptive optics ophthalmoscopy in the human eye. Opt Express. 2011;19(15):14160. https://doi.org/10.1364/OE.19.014160.

49. Jonnal RS, Besecker JR, Derby JC, Kocaoglu OP, Cense B, Gao W, et al. Imaging outer segment renewal in living human cone photoreceptors. Opt Express. 2010;18(5):5257–70.

50. Kocaoglu OP, Liu Z, Zhang F, Kurokawa K, Jonnal RS, Miller DT. Photoreceptor disc shedding in the living human eye. Biomed Opt Express. 2016;7(11):4554. https://doi.org/10.1364/BOE.7.004554.

51. Marcos S, Werner JS, Burns SA, Merigan WH, Artal P, Atchison DA, et al. Vision science and adaptive optics, the state of the field. Vis Res. 2017; https://doi.org/10.1016/j.visres.2017.01.006.

52. Duan A, Bedggood PA, Metha AB, Bui BV. Reactivity in the human retinal microvasculature

measured during acute gas breathing provocations. Sci Rep. 2017;7(1):2113. https://doi.org/10.1038/s41598-017-02344-5.

53. Guevara-Torres A, Joseph A, Schallek JB. Label free measurement of retinal blood cell flux, velocity, hematocrit and capillary width in the living mouse eye. Biomed Opt Express. 2016;7(10):4228. https://doi.org/10.1364/BOE.7.004228.

54. Tam J, Martin JA, Roorda A. Noninvasive visualization and analysis of parafoveal capillaries in humans. Invest Ophthalmol Vis Sci. 2010;51(3):1691–8. https://doi.org/10.1167/iovs.09-4483.

55. Dubra A, Sulai Y, Norris JL, Cooper RF, Dubis AM, Williams DR, et al. Noninvasive imaging of the human rod photoreceptor mosaic using a confocal adaptive optics scanning ophthalmoscope. Biomed Opt Express. 2011;2(7):1864–76. https://doi.org/10.1364/BOE.2.001864.

56. Merino D, Duncan JLJL, Tiruveedhula P, Roorda A. Observation of cone and rod photoreceptors in normal subjects and patients using a new generation adaptive optics scanning laser ophthalmoscope. Biomed Opt. 2011;2(8):2189–201. https://doi.org/10.1364/BOE.2.002189.

57. Roorda A, Williams DR. Optical fiber properties of individual human cones. J Vis. 2002;2(5):404–12. https://doi.org/10.1167/2.5.4.

58. Liu Z, Kurokawa K, Zhang F, Lee JJ, Miller DT. Imaging and quantifying ganglion cells and other transparent neurons in the living human retina. Proc Natl Acad Sci U S A. 2017; https://doi.org/10.1073/pnas.1711734114.

59. Rossi EA, Granger CE, Sharma R, Yang Q, Saito K, Schwarz C, et al. Imaging individual neurons in the retinal ganglion cell layer of the living eye. Proc Natl Acad Sci U S A. 2017; https://doi.org/10.1073/pnas.1613445114.

60. Roorda A, Zhang Y, Duncan JL. High-resolution in vivo imaging of the RPE mosaic in eyes with retinal disease. Invest Ophthalmol Vis Sci. 2007;48(5):2297–303. https://doi.org/10.1167/iovs.06-1450.

61. Scoles D, Sulai YN, Dubra A. In vivo dark-field imaging of the retinal pigment epithelium cell mosaic. Biomed Opt Express. 2013;4(9):1710–23. https://doi.org/10.1364/BOE.4.001710.

62. MacKeben M, Gofen A. Gaze-contingent display for retinal function testing by scanning laser ophthalmoscope. J Opt Soc Am A Opt Image Sci Vis. 2007;24(5):1402–10.

63. Mainster M, Timberlake G, Webb RH, Hughes G. Scanning laser ophthalmoscopy: clinical applications. Ophthalmology. 1982;89:852–7.

64. Webb RH, Hughes GW, Pomerantzeff O. Flying spot TV ophthalmoscope. Appl Opt. 1980; 19(17):2991–7.

65. Cooper RF, Sulai YN, Dubis AM, Chui TY, Rosen RB, Michaelides M, et al. Effects of intraframe distortion on measures of cone mosaic geometry from adaptive optics scanning light ophthalmoscopy.

Transl Vis Sci Technol. 2016;5(1):10. https://doi.org/10.1167/tvst.5.1.10.

66. Timberlake GT, Sharma MK, Gobert DV, Maino JH. Distortion and size calibration of the scanning laser ophthalmoscope (SLO) laser-beam raster. Optom Vis Sci. 2003;80(11):772–7.

67. Poonja S, Patel SS, Henry L, Roorda A. Dynamic visual stimulus presentation in an adaptive optics scanning laser ophthalmoscope. J Refract Surg. 2005;21(1081–597X LA–eng PT–Journal Article SB–IM):S575–80.

68. Rolfs M. Microsaccades: small steps on a long way. Vis Res. 2009;49(20):2415–41. https://doi.org/10.1016/j.visres.2009.08.010.

69. Rucci M, Victor JD. The unsteady eye: an information-processing stage, not a bug. Trends Neurosci. 2015;38(4):195–206. https://doi.org/10.1016/j.tins.2015.01.005.

70. Martinez-conde S, Macknik SL, Hubel DH. The role of fixational eye movements in visual perception. Nat Rev Neurosci. 2004;5(3):229–40. https://doi.org/10.1038/nrn1348.

71. Ratnam K, Domdei N, Harmening WM, Roorda A. Benefits of retinal image motion at the limits of spatial vision. J Vis. 2017;17(1):30. https://doi.org/10.1167/17.1.30.

72. Mulligan JB. Recovery of motion parameters from distortions in scanned images. In: Le Moigne J, editor. Proceedings of the image registration workshop. 1997. p. 281–292.

73. Stetter M, Sendtner R a, Timberlake GT. A novel method for measuring saccade profiles using the scanning laser ophthalmoscope. Vis Res. 1996;36(13):1987–94. 0042-6989(95)00276-6 [pii].

74. Arathorn DW, Yang Q, Vogel CR, Zhang Y, Tiruveedhula P, Roorda A. Retinally stabilized cone-targeted stimulus delivery. Opt Express. 2007;15(21):13731–44.

75. Yang Q, Arathorn DW, Vogel CR, Roorda A. Design of an integrated hardware interface for AOSLO image capture and cone-targeted stimulus delivery. Opt Express. 2010;18(17):17841–58.

76. Sheehy CK, Tiruveedhula P, Sabesan R, Roorda A. Active eye-tracking for an adaptive optics scanning laser ophthalmoscope. Biomed Opt Express. 2015;6(7):2611–22. https://doi.org/10.1364/BOE.6.002412.

77. Domdei N, Domdei L, Reiniger JL, Linden M, Holz FG, Roorda A, Harmening WM. Ultra-high contrast retinal display system for single photoreceptor psychophysics. Biomed Opt Express. 2018;9(1):157. https://doi.org/10.1364/BOE.9.000157.

78. Grieve K, Tiruveedhula P, Zhang Y, Roorda A. Multi-wavelength imaging with the adaptive optics scanning laser ophthalmoscope. Opt Express. 2006;14(25):12230–42.

79. Harmening WM, Tiruveedhula P, Roorda A, Sincich LC. Measurement and correction of transverse chromatic offsets for multi-wavelength retinal microscopy in the living eye. Biomed Opt Express.

2012;3(9):2066–77. https://doi.org/10.1364/BOE.3.002066.

80. Thibos LN, Bradley A, Still DL, Zhang X, Howarth PA. Theory and measurement of ocular chromatic aberration. Vis Res. 1990;30(1):33–49.

81. Marcos S, Burns SA, Prieto PM, Navarro R, De Optica I, De Valde D, Baraibar B. Investigating sources of variability of monochromatic and transverse chromatic aberrations across eyes. Vis Res. 2001;41(28):3861–71.

82. Rynders M, Lidkea B, Chisholm W, Thibos LN. Statistical distribution of foveal transverse chromatic aberration, pupil centration, and angle psi in a population of young adult eyes. J Opt Soc Am A Opt Image Sci Vis. 1995;12(10):2348–57.

83. Winter S, Sabesan R, Tiruveedhula P, Privitera CM, Unsbo P, Lundstrom L, Roorda A. Transverse chromatic aberration across the visual field of the human eye Linda Lundstr o. J Vis. 2016;16(14):1–10. https://doi.org/10.1167/16.14.9.

84. Bruce KS, Harmening WM, Langston BR, Tuten WS, Roorda A, Sincich LC. Normal perceptual sensitivity arising from weakly reflective cone photoreceptors. Invest Ophthalmol Vis Sci. 2015;56(8):4431–8. https://doi.org/10.1167/iovs.15-16547.

85. Sabesan R, Schmidt BP, Tuten WS, Roorda A. The elementary representation of spatial and color vision in the human retina. Sci Adv. 2016;2(9):e1600797. https://doi.org/10.1126/sciadv.1600797.

86. Pallikaris A, Williams DR, Hofer HJ. The reflectance of single cones in the living human eye. Invest Ophthalmol Vis Sci. 2003;44(10):4580–92. https://doi.org/10.1167/iovs.03-0094.

87. Hofer HJ, Singer B, Williams DR. Different sensations from cones with the same photopigment. J Vis. 2005b;5(5):444–54. https://doi.org/10.1167/5.5.5.

88. Tuten WS, Cooper RF, Tiruveedhula P, Dubra A, Roorda A, Cottaris NP, et al. Spatial summation in the human fovea: the effect of optical aberrations and fixational eye movements. BioRxiv. 2018:283119. https://doi.org/10.1101/283119.

89. Tuten WS, Harmening WM, Sabesan R, Roorda A, Sincich LC. Spatiochromatic interactions between individual cone photoreceptors in the human retina. J Neurosci. 2017;37(39):9498–509. https://doi.org/10.1523/JNEUROSCI.0529-17.2017.

90. Sabesan R, Hofer HJ, Roorda A. Characterizing the human cone photoreceptor mosaic via dynamic photopigment densitometry. PLoS One. 2015;10(12):e0144891. https://doi.org/10.1371/journal.pone.0144891.

91. Schmidt BP, Sabesan R, Tuten WS, Neitz J, Roorda A. Sensations from a single M-cone depend on the activity of surrounding S-cones. Sci Rep. 2018b;8(1):8561. https://doi.org/10.1038/s41598-018-26754-1.

92. Schmidt BP, Boehm AE, Foote KG, Roorda A. The spectral identity of foveal cones is preserved in

hue perception. BioRxiv. 2018a:1–20. https://doi.org/10.1101/317750.

93. Domdei N, Reiniger JL, Pfau M, Charbel Issa P, Holz FG, Harmening WM. Histologie im lebenden Auge. Ophthalmologe. 2016; https://doi.org/10.1007/s00347-016-0411-9.

94. Reiniger JL, Domdei N, Pfau M, Müller PL, Holz FG, Harmening WM. Potential of adaptive optics for the diagnostic evaluation of hereditary retinal diseases. Klin Monbl Augenheilkund. 2017;234(3):311–9. https://doi.org/10.1055/s-0043-100631.

95. Choi SS, Doble N, Hardy JL, Jones SM, Keltner JL, Olivier SS, Werner JS. In vivo imaging of the photoreceptor mosaic in retinal dystrophies and correlations with visual function. Invest Ophthalmol Vis Sci. 2006;47(5):2080–92. https://doi.org/10.1167/iovs.05-0997.

96. Hammer DX, Ferguson RD, Bigelow CE, Iftimia NV, Ustun TE, Burns SA. Adaptive optics scanning laser ophthalmoscope for stabilized retinal imaging. Opt Express. 2006;14(8):3354–67.

97. Ferguson RD, Zhong Z, Hammer DX, Mujat M, Patel AH, Deng C, et al. Adaptive optics scanning laser ophthalmoscope with integrated wide-field retinal imaging and tracking. J Opt Soc Am A. 2010;27(11):A265–77.

98. Yoon MK, Roorda A, Zhang Y, Nakanishi C, Wong L-JC, Zhang Q, et al. Adaptive optics scanning laser ophthalmoscopy images in a family with the mitochondrial DNA T8993C mutation. Invest Ophthalmol Vis Sci. 2009;50(4):1838–47. https://doi.org/10.1167/iovs.08-2029.

99. Tuten WS. Cellular functional architecture of the human cone photoreceptor mosaic. Berkeley: University of California; 2014.

100. Wang Q, Tuten WS, Lujan BJ, Holland J, Bernstein PS, Schwartz SD, et al. Adaptive optics microperimetry and OCT images show preserved function and recovery of cone visibility in macular telangiectasia type 2 retinal lesions. Invest Ophthalmol Vis Sci. 2015;56(2):778–86. https://doi.org/10.1167/iovs.14-15576.

101. Tu JH, Foote KG, Lujan BJ, Ratnam K, Qin J, Gorin MB et al. Dysflective cones: visual function and cone reflectivity in long-term follow-up of acute bilateral foveolitis. Am J Ophthalmol Case Rep. 2017;7:14–9. https://doi.org/10.1016/j.ajoc.2017.04.001.

102. Cooper RF, Tuten WS, Dubra A, Brainard DH, Morgan JIW. Non-invasive assessment of human cone photoreceptor function. Biomed Opt Express. 2017;8(11):5098. https://doi.org/10.1364/BOE.8.005098.

103. Hillmann D, Spahr H, Pfäffle C, Sudkamp H, Franke G, Hüttmann G. In vivo optical imaging of physiological responses to photostimulation in human photoreceptors. Proc Natl Acad Sci U S A. 2016;113(46):13138–43. https://doi.org/10.1073/pnas.1606428113.